Zonula occludens-1 and -2 regulate apical cell structure and the zonula adherens cytoskeleton in polarized epithelia

Alan S. Fanning[a], Christina M. Van Itallie[b], and James M. Anderson[b]
[a]Department of Cell and Molecular Physiology and the Lineberger Comprehensive Cancer Center, University of North Carolina at Chapel Hill, Chapel Hill, NC 27599-7545; [b]National Heart, Lung and Blood Institute, National Institutes of Health, Bethesda, MD 20892

ABSTRACT **The structure and function of both adherens (AJ) and tight (TJ) junctions are dependent on the cortical actin cytoskeleton. The zonula occludens (ZO)-1 and -2 proteins have context-dependent interactions with both junction types and bind directly to F-actin and other cytoskeletal proteins, suggesting ZO-1 and -2 might regulate cytoskeletal activity at cell junctions. To address this hypothesis, we generated stable Madin-Darby canine kidney cell lines depleted of both ZO-1 and -2. Both paracellular permeability and the localization of TJ proteins are disrupted in ZO-1/-2–depleted cells. In addition, immunocytochemistry and electron microscopy revealed a significant expansion of the perijunctional actomyosin ring associated with the AJ. These structural changes are accompanied by a recruitment of 1-phosphomyosin light chain and Rho kinase 1, contraction of the actomyosin ring, and expansion of the apical domain. Despite these changes in the apical cytoskeleton, there are no detectable changes in cell polarity, localization of AJ proteins, or the organization of the basal and lateral actin cytoskeleton. We conclude that ZO proteins are required not only for TJ assembly but also for regulating the organization and functional activity of the apical cytoskeleton, particularly the perijunctional actomyosin ring, and we speculate that these activities are relevant both to cellular organization and epithelial morphogenesis.**

Monitoring Editor
Alpha Yap
University of Queensland

Received: Sep 19, 2011
Revised: Dec 12, 2011
Accepted: Dec 16, 2011

INTRODUCTION

Epithelial barriers create the distinct tissue spaces required for proper organ function. The formation and maintenance of these barriers is dependent on a series of cell–cell contacts that circumscribe the apical-lateral margin of each cell, known collectively as the apical junction complex (AJC). This complex includes the adherens junction (AJ), which promotes tissue integrity by establishing a strong adhesive interface between individual cells (Harris and Tepass, 2010), and the tight junction (TJ), which forms a physical barrier to the movement between cells of ions, macromolecules, immune cells, and pathogens (Shen *et al.*, 2011). Both AJ and TJ are intimately associated with the cortical actin cytoskeleton and are functionally regulated by circumferential actomyosin filaments (Hartsock and Nelson, 2008); the dynamic interaction between cell junctions and the cytoskeleton is critical for the morphogenesis of epithelial tissues during development or tissue repair (Baum and Georgiou, 2011) and the maintenance of the barrier in adult organisms (Turner, 2009).

The zonula occludens (ZO) family of cytosolic proteins (ZO-1, -2, and -3) are multi-domain scaffolds that bind directly to the barrier-forming claudin proteins and also interact with other signaling and structural proteins implicated in TJ structure and function (Fanning and Anderson, 2009). Targeted deletion of either ZO-1 or -2 in mice results in relatively late embryonic lethality (Katsuno *et al.*, 2008; Xu *et al.*, 2008). However, ZO-2–deficient chimeras derived from wild-type blastocysts are clearly viable. Furthermore, depletion of either ZO-1 or -2 individually in cultured cells has only subtle effects on

This article was published online ahead of print in MBoC in Press (http://www.molbiolcell.org/cgi/doi/10.1091/mbc.E11-09-0791) on December 21, 2011.

Address correspondence to: Alan S. Fanning (alan_fanning@med.unc.edu).

Abbreviations used: 1p-MLC, 1-phosphomyosin light chain; AJ, adherens junction; AJC, apical junction complex; aPKCζ, atypical protein kinase C ζ; BSA, bovine serum albumin; dKD, double-knockdown; DMP, dry milk powder; EM, electron microscopy; FITC, fluorescein isothiocyanate; GEF, guanine nucleotide exchange factor; GFP, green fluorescent protein; GST-RBD, GTPase-binding domain of Rhotekin; IgG, immunoglobulin G; KD, knockdown; MDCK, Madin-Darby canine kidney; MLC, myosin light chain; Mypt, myosin phosphatase; ROCK, Rho kinase; SEM, scanning electron microscopy; shRNA, short hairpin RNA; TEM, transmission electron microscopy; TER, transepithelial resistance; Tet, tetracycline; TJ, tight junction; Z1Z2, ZO-1/ZO-2; Z2Z1, ZO-2/ZO-1; ZA, zonula adherens.

junction structure and function (Umeda *et al.*, 2004; McNeil *et al.*, 2006; Hernandez *et al.*, 2007). Both observations suggest that there is considerable functional redundancy among ZO proteins, which has made experimental elucidation of ZO protein function technically difficult. However, a seminal study by Umeda and coworkers demonstrated that depletion of both ZO-1 and -2 in cultured epithelial cells completely eliminated TJ barrier formation (Umeda *et al.*, 2006). In ZO-depleted cells, barrier-forming proteins like claudin and occludin were unable to assemble into the characteristic strands normally found in the TJ, indicating ZO proteins are necessary for TJ assembly.

Recent studies suggest that ZO proteins may also have a role in the assembly and/or function of AJs. In both vertebrates and invertebrates they bind to several AJ proteins, including α-catenin, ARVCF, p120, and AF-6/afadin (Itoh *et al.*, 1997; Yamamoto *et al.*, 1997; Takahashi *et al.*, 1998; Wittchen *et al.*, 2003; Kausalya *et al.*, 2004). ZO-1 and -2 are recruited to the punctate AJs that assemble following epithelial cell–cell contact, and only segregate from AJs into nascent TJs as cells polarize (Yonemura *et al.*, 1995; Ando-Akatsuka *et al.*, 1999; Suzuki *et al.*, 2002). They also localize to cadherin-mediated cell–cell adhesions in mesenchymal and neuronal tissues (Ando-Akatsuka *et al.*, 1999; Inagaki *et al.*, 2003; Katsuno *et al.*, 2008) and are ubiquitous components of invertebrate AJs (Wei and Ellis, 2001; Lockwood *et al.*, 2008). Depletion of ZO-1 and -2 in cultured epithelial cells is associated with a delay in the assembly of the belt-like AJ and associated perijunctional actomyosin ring (Ikenouchi *et al.*, 2007). Similarly, loss of ZO proteins in invertebrate epithelia results in disruption of normal epithelial morphogenesis and the cytoskeletal architecture of AJs, although the localization of AJ proteins like cadherin and catenin appears relatively unaffected (Jung *et al.*, 2006; Lockwood *et al.*, 2008; Seppa *et al.*, 2008; Choi *et al.*, 2011). These observations strongly implicate ZO proteins in some aspect of AJ function, although the precise mechanistic role is not understood.

However, one possibility suggested by the observations described above is that ZO proteins regulate the structure and/or function of the cytoskeleton at TJs and AJs. ZO proteins bind directly to F-actin, as well as to many structural and regulatory components of the actin cytoskeleton (Fanning and Anderson, 2009). These include proteins that regulate the assembly and organization of actin filaments (e.g., cortactin, protein 4.1, and α-actinin-4; Mattagajasingh *et al.*, 2000; Chen *et al.*, 2006; Kremerskothen *et al.*, 2011), those that regulate myosin II activity (e.g., Shroom2 and MRCKβ; Etournay *et al.*, 2007; Huo *et al.*, 2011), and those that regulate Rho-GTPase signaling, such as the cdc42 guanine nucleotide exchange factor (GEF) Tuba and paracingulin (Otani *et al.*, 2006; Pulimeno *et al.*, 2011). Studies to date support the hypothesis that ZO proteins regulate the recruitment of actin and myosin II into the circumferential AJ during the early events of junction assembly in cultured cells (McNeil *et al.*, 2006; Ikenouchi *et al.*, 2007; Yamazaki *et al.*, 2008). However, the extent to which ZO proteins regulate cytoskeletal organization in later steps of junction assembly, and how this might affect the steady-state structure and function of AJs and TJs, is still poorly understood.

To better understand how ZO proteins regulate the structure and function of the AJC in fully polarized epithelial cells, we have established Madin-Darby canine kidney (MDCK) II cell lines in which both ZO-1 and -2 have been depleted. We confirmed the requirement for ZO proteins in TJ assembly and barrier formation. In addition, we observed a striking expansion of contractile actomyosin arrays associated with the AJ in ZO-deficient cells. This expansion is associated with changes in cell shape, the organization of cells within the epithelium, and the structure of the apical plasma membrane. These observations suggest that ZO proteins regulate the assembly and contractility of the AJ cytoskeleton and apical cell shape, and provide the first evidence that the structure of the AJC may be synergistically regulated by interactions between AJs and TJs through ZO proteins.

RESULTS

The levels of all three ZO proteins are decreased in MDCK II Tet-Off cells stably transfected with ZO-1 and ZO-2 short hairpin RNA constructs

To assess the functional role of ZO proteins in epithelial organization, cell structure, and barrier formation we established stable MDCK Tet-Off cell lines expressing short hairpin RNA (shRNA) sequences targeting both ZO-1 and -2. In three independently isolated clones, ZO-1 expression was reduced by over 97%, while ZO-2 expression was almost undetectable (Figure 1A). In addition, although ZO-3 expression was not directly targeted, expression in all three double-knockdown (dKD) lines was reduced by more than 60%. ZO-1 (Figure 1A) and -2 (unpublished data) expression could be effectively restored by expression of a recombinant myc-tagged ZO-1 rescue transgene (ZO1R). Restoration of either ZO-1 or -2 was also sufficient to restore ZO-3 expression to normal levels (Figure 1A). This decrease in expression of the three ZO proteins was confirmed by immunocytochemistry (Figure 1B). Close observation of the small amount of residual staining of ZO-1 and -3 in the dKD epithelia revealed that the normal jagged pattern of cell–cell contacts characteristic of MDCK II cell TJs is much more linear, and overall cell shape in dKD cells is more polygonal.

These changes in ZO protein expression had corresponding effects on some, but not all, other proteins that normally localize to TJs and bind directly to ZO-1. For example, the localization of both the transmembrane protein occludin and the cytoplasmic scaffolding protein cingulin were reduced at the TJ (Figure 2A). In contrast, the distributions of the occludin paralogue tricellulin and the cell adhesion molecule JAM-A were unaltered (Figure 2A). Similarly, while the accumulation of claudin-1 and -2 at the AJC was reduced relative to control cells, that of claudin-3 and -4 appeared normal (Figure 2B). However, as noted above, the distribution of all proteins in the AJC was much more linear in dKD cells than in control MDCK cells, which characteristically have wavy cell junctions. These shape changes were most obvious in an ~1-μm-thick section that contained the AJC, and were not noticeable in more basal aspects of the epithelium (unpublished data). In spite of clear alterations in distribution, the expression levels of these proteins in dKD and control cells were not different (Supplemental Figure S1A). Changes in the distribution of occludin and claudin-2 in dKD cells could be rescued by tetracycline (Tet)-induced expression of ZO1R (Figure S1B), as could the changes in junction contour and cell shape. These results confirm the previous observation (Umeda *et al.*, 2006) that ZO proteins are required for the localization of other TJ proteins and further suggest that ZO proteins play a role in determining the shape of cell contacts.

The paracellular barrier is selectively perturbed in ZO dKD epithelia

The movement of solutes through the TJ is both charge and size selective (Anderson and Van Itallie, 2009). Solutes smaller than 4 Å in radius, including ions, pass through high-permeability, charge-selective, claudin-based pores, while larger solutes pass with much lower permeability through the so-called "leak pathway." Transepithelial resistance (TER) measures conductance through the claudin pores,

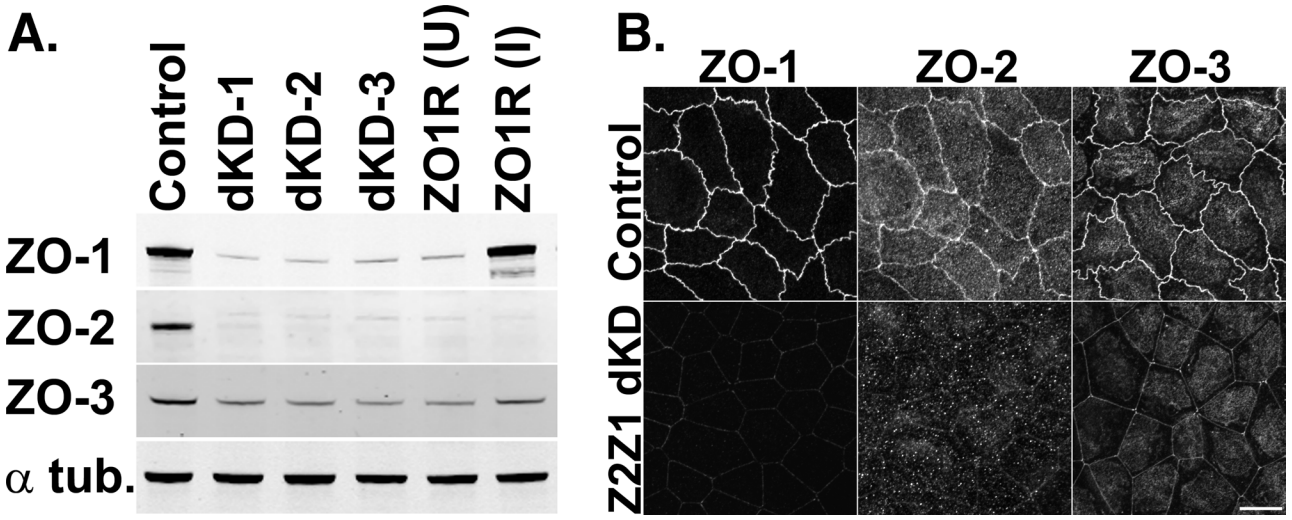

FIGURE 1: ZO-1 and -2 are effectively depleted in stable MDCK II Tet-Off cell lines. (A) Western blot of ZO-1, -2, and -3 polypeptides in control, dKD (lines 1–3), and in dKD cells expressing a Tet-inducible full-length ZO-1 rescue transgene (ZO1R). ZO-1 expression in dKD lines is ~2–3% of that observed in control cells, while ZO-2 expression is almost undetectable. Note that ZO-3, while not directly targeted in dKD cells, is also reduced by up to 50%. In ZO1R cell lines, induction of ZO1R (I) restores ZO-1 and ZO-3 expression to levels equivalent to those in control cells, while ZO-2 expression remains suppressed. U, uninduced; I, induced. (B) Immunocytochemistry of ZO-1, -2, and -3 in the control and dKD-3 cell line. There is a dramatic reduction in the staining of all three peptides at the AJC, and the outline of the AJC is much more trapezoidal in dKD cells relative to control cells. All images are 1-μm-thick, maximum-density projections of the AJC. Scale bar: 10 μm.

while the flux of larger solutes is measured over much longer time intervals and is thought to reflect the stability or dynamics of cell–cell contacts (Shen *et al.*, 2011). Despite the dramatic decrease in ZO protein levels and the altered distribution of many TJ proteins, we found that TER was not significantly different in three dKD lines relative to control cells (Figure 3A). There was a small, but significant, decrease in the dilution potential of dKD epithelia (Figure 3B), which measures the charge selectivity of the junction. This was due to a relative increase in chloride conductance (Figure S2A) relative to sodium (Figure S2B), presumably due to the change in the ratio of claudins in the barrier, as documented by immunofluorescence localization (Figure 2). These changes were reversed by expression of ZO1R. Thus the barrier to ions is relatively unperturbed in ZO-depleted MDCK cells.

In contrast to TER, the barrier to large solutes through the leak pathway is dramatically reduced. Control monolayers normally show clear size discrimination for polyethylene glycol (PEG) oligomers with a cutoff above ~4 Å radius (Figure 3C). This discrimination was lost in ZO-depleted cells, and the apparent permeability of all size classes, up to 7 Å radius, was dramatically increased (Figure 3C). The flux of 3-kDa fluoresceinated dextran (radius of 17 Å) demonstrated a similar large (~20-fold) increase in permeability (Figure 3D), which could be partially reversed in dKD cells by expression of ZO1R. Thus depletion of ZO proteins in MDCK II cells has a specific effect on the movement of large solutes measured over relatively long time intervals (>2 h), but has little effect on the movement of small ions through the claudin pores when measured at intervals <1 s using TER.

We also observed that the kinetics of barrier assembly and disassembly were dramatically altered in dKD monolayers, as assessed using the calcium-switch (Ca^{2+}-switch) assay (Martinez-Palomo *et al.*, 1980). dKD monolayers lost their electrical barrier much more rapidly than control or single-knockdown (KD) epithelia after calcium removal (Figure S2C) and regained a barrier much more slowly when calcium was restored (Figure S2D). The enhanced permeability for large solutes and the altered barrier assembly/disassembly kinetics in the Ca^{2+}-switch assay may reflect both alterations in the stability of cell–cell contacts in dKD monolayers and changes in the steady-state dynamics of TJ proteins.

The AJC cytoskeleton is dramatically reorganized in ZO-depleted cells

Changes in epithelial permeability and TJ structure following pathological or pharmacological intervention are often associated with changes in the cytoskeleton at the AJC, and ZO proteins are notable for their direct and indirect contacts with the cortical cytoskeleton. To determine to what extent ZO proteins might be required for cytoskeletal organization of the AJC, we examined the distribution of actin and myosin IIB in control and dKD cells. In control cells, the F-actin associated with the AJC is concentrated into a thin band that circumscribes the apical margin of the cell and highlights the wavy cell junctions (Figure 4A). The staining of myosin IIB follows that of actin but appears somewhat more punctate and is more concentrated at the tricellular junctions. There is also a diffuse staining of both proteins in the apical domain that probably represents the terminal web and brighter puncta from the sparse microvilli that are characteristic of these cells.

The apical actomyosin organization is dramatically altered in ZO-depleted cells (Figure 4A). Myosin IIB and F-actin are recruited into large arrays just inside the AJC that follow the straight contour of the cell–cell contacts. Myosin IIB shows a punctate distribution with a 400- to 600-nm repeat that often, but not always, appears to be aligned in adjacent cells. There are also large aggregates of actin and myosin staining associated with the apical surface (Figure 4A). In contrast, the distribution of actin and myosin IIB in the lateral domain (unpublished data) and the organization of stress fibers on the basal (substrate-attached) domain are apparently unaffected

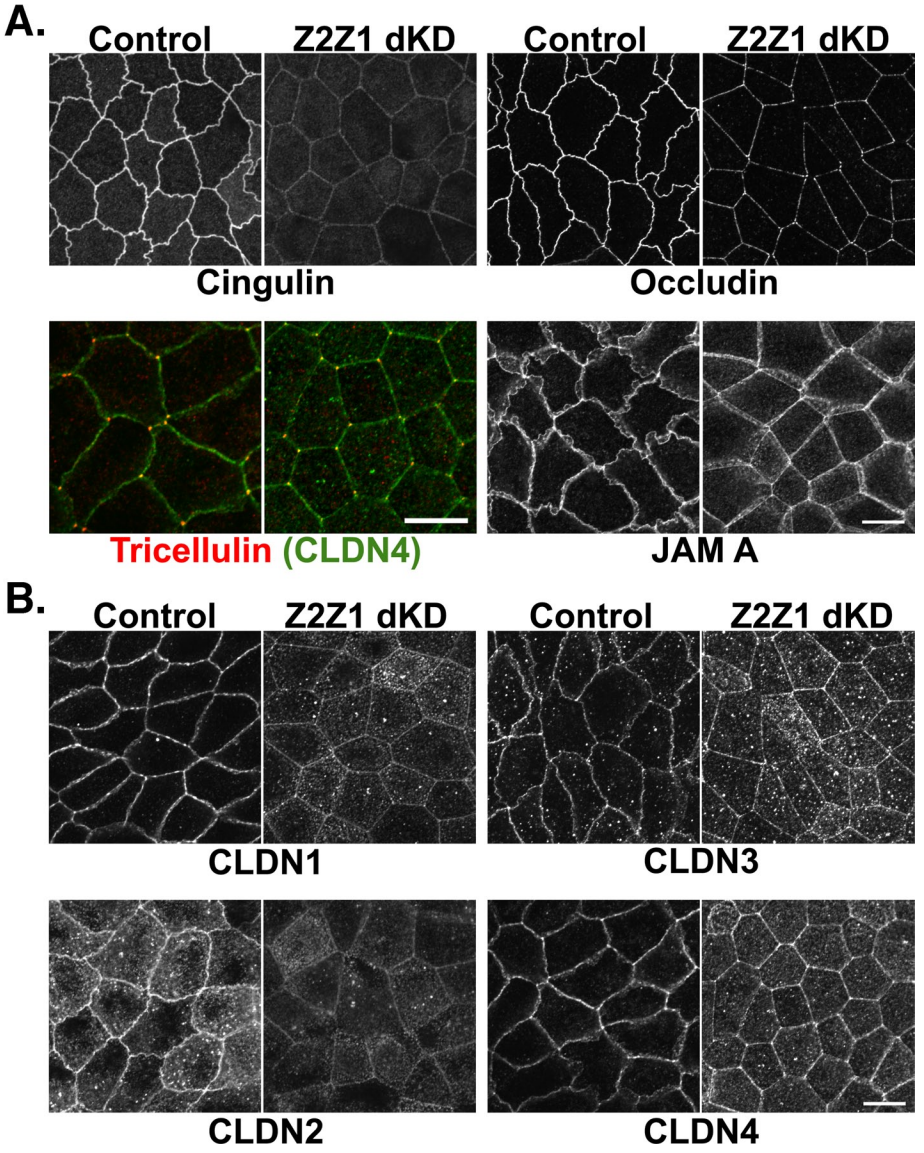

FIGURE 2: The localization of some, but not all, TJ proteins to the AJC is attenuated in ZO dKD cell lines. (A–C) A 1-μm-thick, maximum-density projection of the apical domain, en face, acquired at the AJC (see *Materials and Methods*). (A) Occludin and cingulin localization at the AJC is reduced, whereas JAM-A and tricellulin appear relatively normal in dKD cells relative to control cells. Claudin-4 staining (green) is included with tricellulin staining (red) to highlight tricellular junctions. (B) Claudin-1 and -2 staining at the AJC is reduced, whereas claudin-3 and -4 appear relatively normal in dKD cells. Note again the dramatic change in cell shape at the AJC in dKD cells. Scale bar: 10 μm.

(Figure 4B). Myosin IIA shows a similar distribution to myosin IIB in dKD cells (Figure S3), although we noted that myosin IIA does not appear to be enriched in the AJC in control cells. There were no changes in the steady-state accumulation of any of the cytoskeletal proteins examined (actin, myosin II, and Rho kinases [ROCKs]; Figure S4). Changes in the distribution of F-actin and myosin II in ZO-depleted cells, and the accompanying changes in cell shape, could be rescued by Tet-induced expression of ZO1R (Figure S5A). The changes in F-actin distribution and cell shape were evident at the earliest time points examined after Ca^{2+}-switch (Figure S5B). Thus these observations reveal a dramatic expansion of the cytoskeleton at the AJC in ZO-depleted cells.

Ultrastructural analysis of control and dKD cells by transmission electron microscopy (TEM) confirmed that the expanded arrays of F-actin in dKD cells assemble adjacent to the plasma membrane (Figure 5). In normal MDCK II cells, the circumferential actomyosin ring appears as a small accumulation of electron-dense actin at the AJ, which is below the region of close membrane apposition at the TJ (Figure 5A). These points of cell contact, sometimes called "kisses," are still evident in ZO-depleted cells (Figure 5B, arrow), consistent with the presence of the functional ion barrier described above. We have also observed that freeze-fracture strands, characteristic of TJs, are found in both control and ZO-depleted cells (Figure S6). In dKD cells, there is a striking accumulation of F-actin at the plasma membrane below the TJ kisses (Figure 5B, brackets) in the region normally associated with the AJ. In sections tangential to the AJC, the filamentous actin in control cells appears to be loosely associated with wavy cell–cell contacts (Figure 5C), while actin filament arrays in dKD cells are much larger and run parallel to the straight cell–cell contacts (Figure 5D). Thus ZO depletion in MDCK II cells caused a marked accumulation of highly organized actin filaments specifically at AJs.

ZO depletion alters the morphology of the apical domain and the organization of cells within the epithelium

To better understand the organization of control and dKD cells within an epithelium we examined low-magnification electron microscopy (EM) cross-section images of cells grown on Transwell filter inserts. MDCK II cells at steady state form a highly ordered array of densely packed cuboidal cells that are ~4 μm tall, as measured from basal lamina to AJC (Figure 6A, Control). Scanning EM (SEM) analysis indicates that these cells have a relatively flat apical domain sparsely populated with individual microvilli that sometimes form small clumps (Figure 6B, Control). ZO-depleted cells are noticeably less uniform in their epithelial packing, and are much taller than control cells: ~7 μm from basal lamina to AJC (Figure 6A, Z2Z1 dKD). ZO dKD cells are packed such that they "lean" or "twist" around adjacent cells, with their bases being misaligned from their apical domains, but they do not appear to multilayer. Both TEM and SEM indicate there is a dramatic distension in the apical surface of many dKD cells, with numerous long, microvilli-like structures (Figure 6, A and B). Interestingly, these distensions do not appear to begin at cell–cell contacts, but instead begin ~3–5 μm from the point of cell–cell contact. This is most clear in the SEM images (Figure 6B).

Despite these dramatic changes in cell structure, Z-section immunofluorescence analysis indicates that the overall polarity of plasma membrane markers appears to be maintained in dKD cells (Figure 7A). Apical markers like gp135/podocalyxin and ezrin are still restricted to the apical surface, although the apical distortion

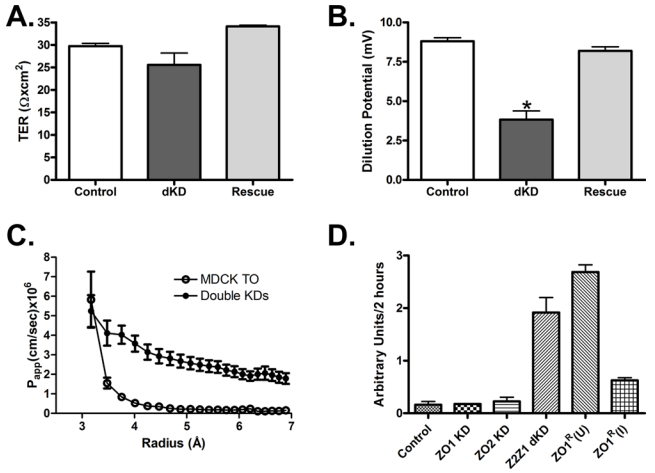

FIGURE 3: The paracellular barrier in dKD cells is selectively perturbed. (A) The TER is maintained in dKD cells, and is unaffected by expression of the full-length ZO-1 transgene. (B) The dilution potential of the dKD cell lines is significantly reduced, but is reversed by expression of the full-length ZO-1 rescue transgene. (C) Size selectivity of the paracellular barrier is measured by the paracellular movement of a graded series of PEG oligomers from 2.6–7.0 Å radius. The size selectivity of these uncharged solutes is lost in dKD cell. (A–C) n = 3 clones. (D) The flux of 3-kDa FITC-dextran is dramatically increased in dKD and uninduced (U) ZO1R epithelia relative to control or ZO-1 or -2 single-KD cell lines. The increased flux is partially reversed by expression (I) of ZO1R.

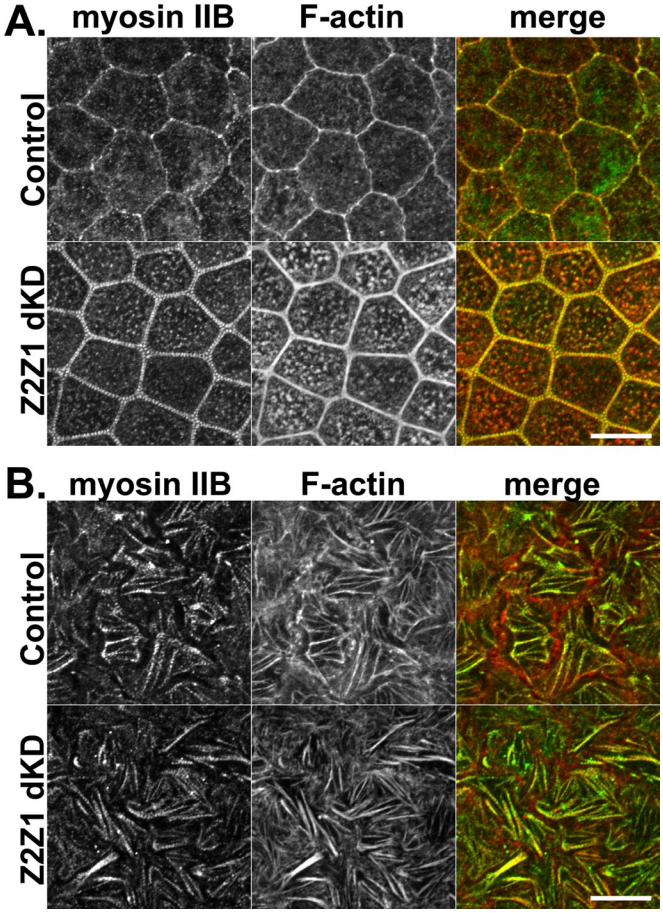

FIGURE 4: There is a dramatic reorganization of the cytoskeleton within the AJC. (A) Control and dKD cells were fixed and stained with TRITC-phalloidin (F-actin) and antibodies against myosin IIB, and the acquired images are presented as a 1-μm-thick, maximum-density projection of the AJC. In dKD cells, the cell–cell contacts at the AJC are more linear, cell shape is more trapezoidal, and F-actin and myosin IIB are reorganized into a thick array of fibrils with a 400–600 Å repeat of myosin IIB. There are also distinct foci of F-actin and myosin IIB within this apical section of dKD cells that are not apparent in control cells. (B) The organization of F-actin and myosin IIB in a 1-μm-thick, maximum-density projection of the basal (substrate-associated) domain appears relatively normal. Scale bar: 10 μm.

evident in ultrastructural analysis is reflected in their distribution. Interestingly, the transmembrane glycoprotein gp135 appears to concentrate within the apical extension, while the cytosolic scaffolding molecule ezrin is distributed throughout the apical domain (Figure 7A). The AJ markers α- and β-catenin are restricted to the lateral domain of dKD cells, as they are in control cells, although the changes in cell packing observed above are obvious from their distribution. Indeed, all of the markers tested demonstrated an appropriately polarized distribution. Finally, the polarity determinants PAR-3 (Figure 7A), Lgl2, and atypical protein kinase C ζ (aPKCζ; unpublished data) are still localized to the appropriate domains. These observations confirm that cell polarity is still intact in ZO-depleted cells, despite significant reorganization of the perijunctional cytoskeleton and apical membrane structure.

Similarly, depletion of ZO proteins does not disrupt the inherent ability of MDCK II cells to form organized cystic structures in a three-dimensional collagen culture assay. Over 80% of the cysts formed by ZO-depleted cells (352/416) plated in a collagen matrix had a single large lumen, compared with ~60% (101/170) of control cells (Figure 7B). However, the lumens of these cysts formed by ZO-depleted cells contained a phase-dense material that stained positive for the apical marker gp135/podocalyxin. Furthermore, there were numerous indentations (Figure 7B, arrowhead) and distensions (Figure 7B, arrow) of the apical/luminal surface that stained with both gp135 and F-actin. These changes to apical surface are similar to those observed in cells plated on plastic, that is, in two-dimensional culture (Figure 6). Thus, while some of the morphological changes observed in two-dimensional culture are also observed in three-dimensional culture (e.g., altered apical surface morphology), ZO-depleted cells are still able to create cysts with a single lumen. Future studies will determine to what extent the other cytoskeletal and morphological changes seen in two-dimensional culture occur in three-dimensional culture.

ZO depletion does not affect the localization of AJ proteins

In polarized epithelial cells, the cell adhesion molecules of the cadherin–catenin complex are closely associated with the circumferential band of F-actin at the AJ. In MDCK II cells, they are also more generally distributed along the lateral surface. Despite the dramatic changes in actin and myosin organization in dKD cells, we could detect few changes in the distribution (Figure 8) or steady-state expression (Figure S7B) of the core components of the cell adhesion complex: E-cadherin and α-, β-, and p120 catenin. Nor did we detect any changes in the kinetics of E-cadherin localization to cell–cell contacts following Ca^{2+}-switch (Figure S5B). We conclude that the large increase in actin localization at the zonula adherens (ZA; Figure 4A) in ZO-depleted cells does not alter the assembly or steady-state distribution of the core AJ proteins. These observations suggest that the steady-state localization of these proteins in polarized cells can be maintained independent of ZO proteins, and that the accumulation of actomyosin at the AJ does not necessarily lead to an increased accumulation of AJ proteins.

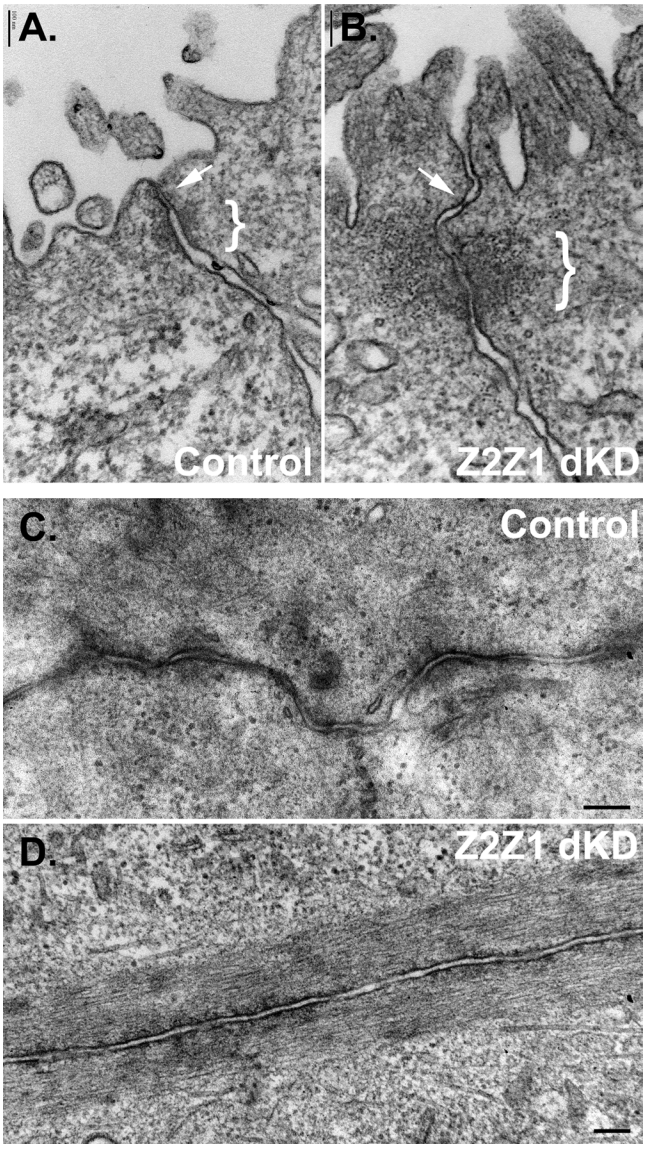

FIGURE 5: F-actin forms large parallel arrays adjacent to the plasma membrane at the most apical aspect of the lateral domain. (A and B) TEM cross-sections of control (A) and dKD (B) MDCK cells at the apical domain. Note the increased electron density at the lateral membrane (brackets), almost immediately below the microvilli, in dKD cells relative to control cells. Note also that membrane contacts, or "kisses," characteristic of TJs are still observed in dKD cells (arrows). (C and D) En face section of control (C) and dKD (D) epithelial monolayers. There are large parallel filaments in dKD (D) cells that are never observed in control cells. Scale bars: (A and B) 100 nm; (C and D) 200 nm.

Actin and myosin form a contractile array in ZO-depleted cells

The perijunctional actomyosin ring associated with the AJ is thought to be a contractile array that generates tension within the AJC (Mooseker, 1976). To examine whether ZO depletion triggers apical contraction, we diluted ZO-depleted cells marked with green fluorescent protein (GFP) into MDCK II cells and measured the apical area of dKD cells relative to adjacent wild-type cells (Figure 9A). We observed that the apical diameter of GFP-marked dKD cells (Figure 9A, arrows) was consistently smaller than the basal diameter, and the cells had a distinctive cone-shaped appearance in maximum-density *z*-axis projections. The mean apical area of ZO-depleted cells (64.7 ± 29.6 μm^2; n = 18) was consistently smaller than surrounding wild-type cells (142.4 ± 48.1 μm^2; n = 103), consistent with apical contraction (Figure 9B). We also looked at the distribution of markers commonly associated with the activation of actomyosin contraction. We found that both ROCK-1 and 1-phosphomyosin light chain (1p-MLC), the active form of myosin light chain (MLC), are much more concentrated at the AJC in ZO-depleted cells relative to control cells (Figure 9C). In fact, we detected little, if any, 1p-MLC in the AJC of control cells. The changes in subcellular localization of these proteins in dKD cells were not accompanied by changes in the expression levels of ROCK-1 (Figure S4), total MLC, or 1p-MLC (Figure 9D), suggesting that ZO depletion causes a redistribution of these proteins without altering protein levels.

The activity of ROCK-1, and the activation of actomyosin contractility, are often regulated by the RhoA-GTPase signaling pathway, and the activity of this GTPase has been previously implicated in both TJ and AJ assembly and function. However, we saw no increase in the steady-state levels of activated (GTP-bound) RhoA in dKD cells relative to control or ZO-1 single-KD cells (Figure 9E). Furthermore, there was no change in the localization of the RhoA regulators GEF-H1 and paracingulin to the TJ in ZO-depleted cells (unpublished data). We also saw no changes in the levels of phosphorylated myosin phosphatase (Mypt1; Figure S4). Mypt1, like MLC, is a target of ROCK that regulates nonmuscle myosin contractility.

These observations do not rule out the possibility of localized increases in RhoA activity within the AJC, nor do they conclusively prove that the downstream effectors like ROCK and Mypt are not involved in the regulation of AJ actin in ZO-depleted cells. ROCK activity, for example, is regulated by several other signaling pathways. To determine the precise role of ROCK in reorganization of actomyosin observed in ZO-depleted cells, we treated both control and dKD cells with the ROCK inhibitor Y-27632. Stress fiber arrays on the basal surface of both control and ZO-depleted cells were dramatically disrupted by Y-27632 (unpublished data), confirming the efficacy of the ROCK inhibitor in these cells. In control cells, both cell shape and the distribution of actin and myosin IIB in the AJC appeared similar following treatment with either vehicle or Y-27632, and there were no obvious signs of cytoskeletal disruption within the apical domain. In contrast, we found that ROCK inhibition had noticeable effects on the distribution of F-actin and myosin IIB in the apical domain of ZO-depleted cells (Figure 10A); in the region immediately beneath the apical plasma membrane, myosin-IIB staining became more diffuse, and F-actin was organized into a large ring. However, ROCK inhibition only partially reversed the assembly of the actomyosin arrays associated with the AJC. Nor did it reverse the changes in cell shape and junction "linearity." Thus, while ZO depletion does appear to alter the sensitivity of apical cytoskeleton to disruption of ROCK activity, ROCK activity does not appear to be the only factor controlling cytoskeletal reorganization in dKD cells.

Instead, we found the assembly and/or maintenance of the ZA actin in both control and ZO-depleted cells to be highly dependent on the enzymatic activity of myosin II. Control and ZO-depleted cells were treated with vehicle or the myosin II ATPase inhibitor blebbistatin, and the distribution of actin and myosin IIB were determined by immunocytochemistry. Blebbistatin treatment of ZO-depleted cells caused a dramatic reversal of the dKD phenotype. The accumulation of F-actin at the AJC was markedly reduced in blebbistatin-treated cells relative to vehicle-treated dKD cells (Figure 10B), and myosin IIB staining was diminished and accumulated in small

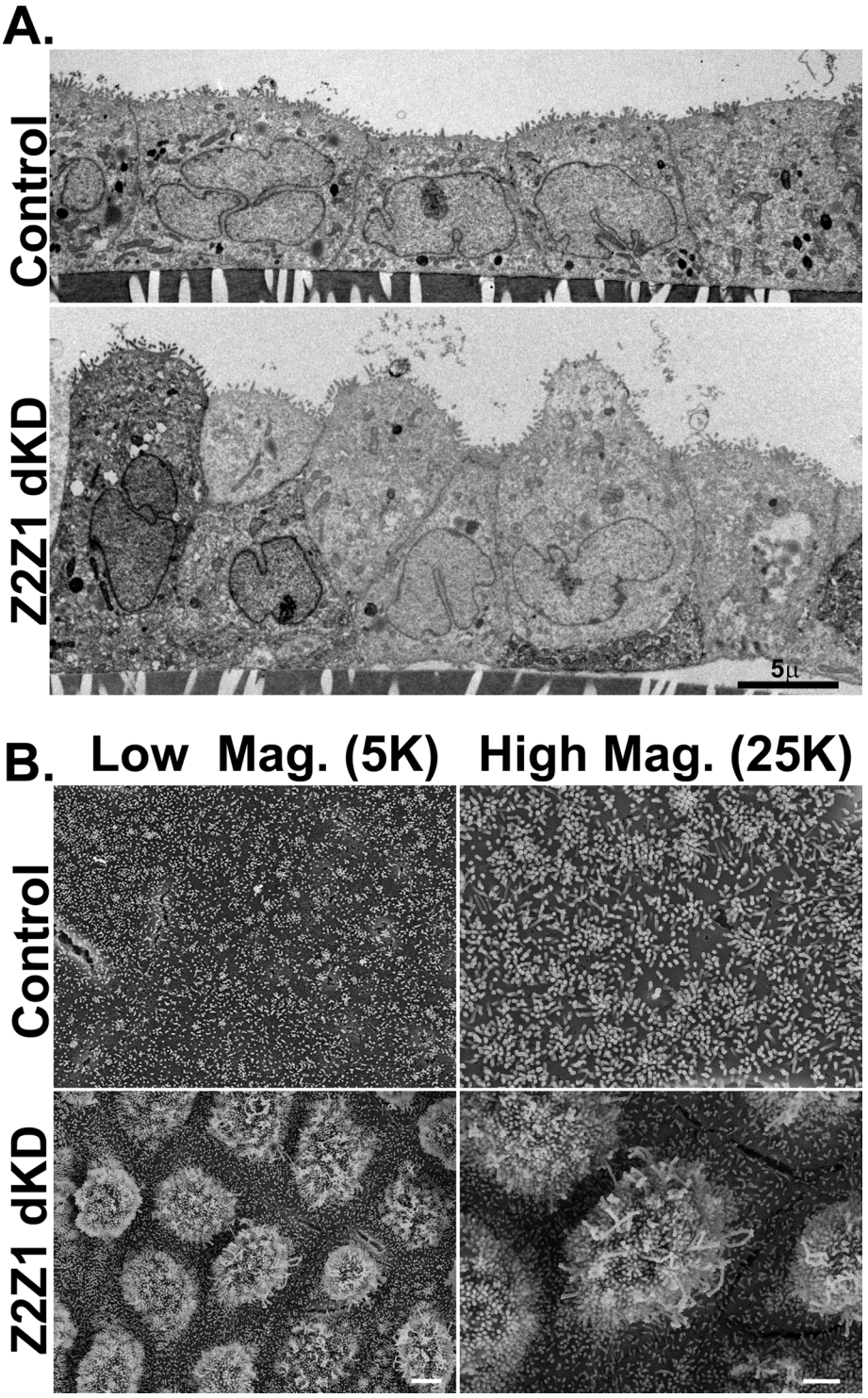

FIGURE 6: The morphology of the apical domain is distorted in ZO dKD cells. (A) TEM of a cross-section of epithelia formed by control and dKD cells. dKD cells are taller when measured from substrate to the AJC, irregularly packed, and often have a distortion of the apical plasma membrane. Scale bar: 5 μm. (B) SEM of control and dKD cells. The distortion of the apical plasma membrane is immediately apparent, and there are long membrane extensions that are distinct from the microspikes normally apparent on the apical domain of control cells. Scale bars: 5 μm (low mag.); 1 μm (high mag.).

irregular puncta. Cell–cell contacts, revealed by actin and myosin IIB staining, were also less linear, and cell shape overall was more rounded. However, cell contacts did not revert to the more undulating appearance characteristic of untreated control cells.

In fact, the distribution of actin and myosin IIB in the AJC of blebbistatin-treated control cells was almost identical to that seen in treated dKD cells. In control cells treated with blebbistatin, the wavy cell–cell contacts characteristic of MDCK II cells were absent, and blebbistatin treatment resulted in a rounding and smoothing of the apical contours similar to that seen in treated dKD cells. Notably, despite the dramatic changes in ZA cytoskeleton and cell structure in blebbistatin-treated cells, there were no significant changes in the flux of 3-kDa dextran in either control or ZO-depleted cells (Figure S8). The flux of dextran through the leak pathway was still dramatically increased in ZO-depleted cells relative to control cells and was not reversed by inhibition of myosin activity and disruption of the ZA actin. This observation suggests that actomyosin activity, particularly in the ZA, is not responsible for the changes in permeability seen in ZO-depleted cells. However, our observations overall indicate myosin II ATPase activity is a critical component of both normal cell shape and junction structure. Our data are also consistent with the hypothesis that ZO proteins are critical regulators of cell shape and ZA contractility, and suggest a mechanism whereby ZO proteins negatively regulate actomyosin activity at cell junctions.

DISCUSSION

Our studies highlight a new aspect of the synergistic relationship among components of the AJC: the TJ, the AJ, and the perijunctional actomyosin ring. Previous studies have demonstrated that cadherin-mediated cell–cell adhesion triggers cytoskeletal assembly and that the cytoskeleton in turn regulates the stability of these adhesive contacts and their expansion into an apical circumferential contact (reviewed in Niessen *et al.*, 2011). They have also demonstrated that cadherin-based cell–cell adhesion and the actin cytoskeleton are either directly or indirectly required for TJ assembly (Gumbiner *et al.*, 1988; Capaldo and Macara, 2007; Kremerskothen *et al.*, 2011). It has been less clear whether TJs themselves actively promote the organization of AJ or the cytoskeleton of the AJC. Our study reveals that ZO proteins in fully polarized cells regulate the assembly and contractility of the perijunctional actomyosin ring associated with the AJ. The depletion of ZO proteins is associated with a dramatic expansion and increased contractility of the perijunctional actomyosin ring, increased cell height, dramatic expansion of the apical plasma membrane, and altered cell packing within the monolayer. These observations suggest that ZO proteins play a role in the morphogenetic processes that regulate epithelial organ development and repair.

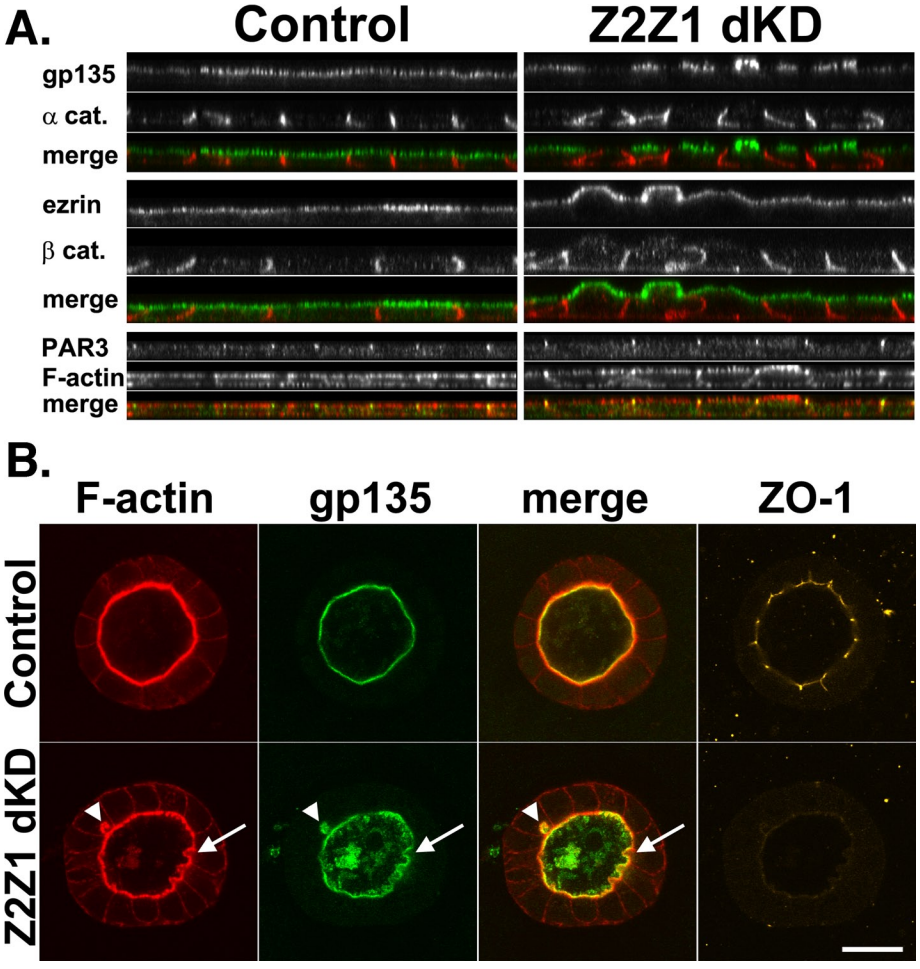

FIGURE 7: ZO-depleted cells have normal cell polarity and form cysts with a single lumen in three-dimensional collagen culture. (A) Confocal Z-section reconstruction of control and dKD cells fixed and stained with antibodies against apical (gp135, ezrin), lateral (α-, β-catenin), and cell polarity (PAR3) markers. The polarized distribution of all markers is maintained, although the apical distortion and altered cell packing are readily apparent. (B) Confocal section through cysts cultured from single cells plated in a collagen suspension. Cysts were fixed and stained with rhodamine-phalloidin and antibodies against the apical marker gp135 and ZO-1. Indentations (arrowheads) and distensions (arrow) of the apical plasma membrane are apparent in dKD cells. Scale bar: 20 μm.

ZO proteins inhibit the assembly and contractility of actomyosin in the AJC

The shape/morphology of the AJC can differ considerably among cultured cell lines. For example, cell junctions in MDCK II cells have a "relaxed" or nonlinear shape, whereas cell junctions in Caco-2 and Eph4 cells tend to have more linear organization (Otani *et al*., 2006). Recent studies have identified several factors that regulate the morphology and contractility of the AJC. For example, overexpression of either the AJC-associated scaffold protein Shroom3 (Hildebrand, 2005) or the FERM-domain protein Lulu (Nakajima and Tanoue, 2010), or depletion of the FERM-domain protein Willin/FRMD6, induce apical constriction in polarized epithelial cells (Ishiuchi and Takeichi, 2011). Similarly, depletion of the cdc42 GEF Tuba can transform the AJC of Caco-2 cells from a linear/constricted morphology to a more relaxed shape, similar to that seen in MDCK II cells (Otani *et al*., 2006). Interestingly, both Tuba and Shroom2 bind to ZO-1, and ZO-1 is required for the localization of Tuba to the AJC (Otani *et al*., 2006; Nishimura and Takeichi, 2008). The expansion and marked contraction of the perijunctional actomyosin ring in ZO-depleted cells suggests that ZO proteins normally inhibit the activity of these proteins, perhaps spatially regulating their activity within the AJC.

The driving force behind apical constriction is the activity of nonmuscle myosin II, which is critical for the assembly and maintenance of the ZA (Ivanov *et al*., 2004, 2005; Smutny *et al*., 2010). In ZO dKD cells, the myosin inhibitor blebbistatin reverses apical constriction, consistent with a role for ZO-1 in either directly or indirectly regulating myosin II activity. Several of the proteins that regulate apical constriction, such as Shroom3, Lulu, and Willin do so by regulating the activity or localization of ROCK, which activates myosin II by phosphorylation of the regulatory light chain. For example, Shroom3 localizes ROCK to the AJC (Nishimura and Takeichi, 2008), while Willin coordinates the aPKC-mediated phosphorylation and inactivation of ROCK (Ishiuchi and Takeichi, 2011). These observations suggest that ROCK is a critical effector of apical constriction. However, in ZO-depleted cells, ROCK inhibition only partially reverses the contractile phenotype observed in ZO dKD cells, suggesting that ZO-1 or -2 may also regulate ROCK-independent pathways that play a role in apical constriction. One possibility is that they do this by modifying the activity of regulatory GEFs such as Tuba, which controls apical constriction through ROCK-independent pathways involving the cytoskeletal regulator neural Wiskott-Aldrich syndrome protein (Otani *et al*., 2006). Alternatively, ZO proteins may regulate apical actin dynamics by direct interaction with cytoskeletal proteins such as cortactin, α-catenin, or α-actinin-4 (Itoh *et al*., 1997; Chen *et al*., 2006). While the mechanisms are still unclear, they are likely to occur during the earlier phases of junction assembly; the changes in cytoskeletal structure observed in ZO-depleted cells are apparent within 2 h of calcium-induced junction assembly (Figure S5B).

While our report focuses on the role of ZO proteins in the steady-state structure of the AJ, these proteins are also likely to have a role earlier in AJ assembly. ZO-1 and -2 colocalize with the cadherin–catenin complex in the punctate AJ that form at nascent cell–cell contacts, and remain associated with these proteins as they are reorganized into the expanding adhesive contact (Ando-Akatsuka *et al*., 1999; Suzuki *et al*., 2002; Tsukita *et al*., 2009). A study by the Tsukita group using ZO-1 (knockout)/ZO-2 (KD) Eph4 cells, a mouse mammary epithelial line, demonstrated that the initial formation of punctate AJ following calcium depletion/repletion (Ca^{2+}-switch) was apparently normal in these cells, suggesting the ZO proteins are not required to establish these early cell–cell contacts (Ikenouchi *et al*., 2007; Yamazaki *et al*., 2008). However, the expansion of this structure and recruitment of actomyosin into a belt-like AJ was delayed (Ikenouchi *et al*., 2007). Furthermore, in fully confluent ZO-1 (knockout)/ZO-2 (KD) Eph4 cells, there is a

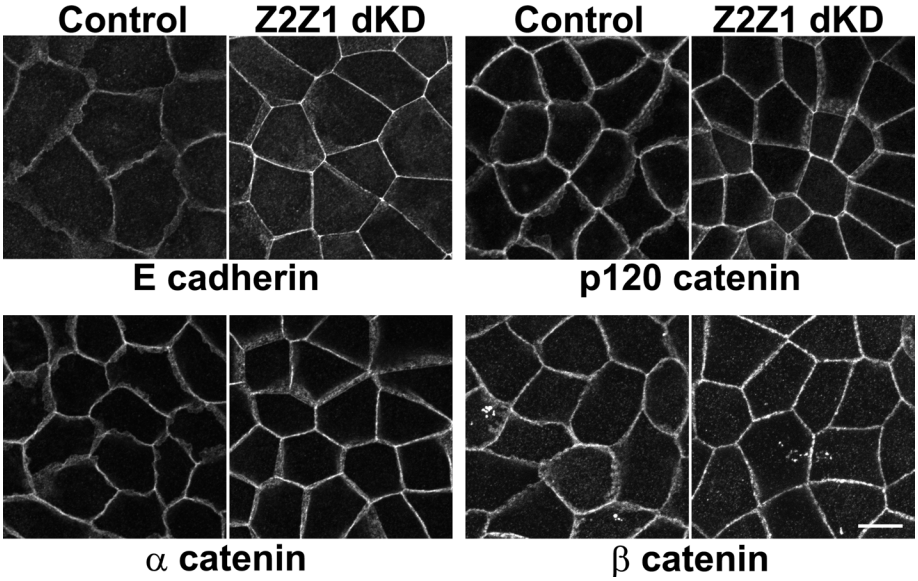

FIGURE 8: The localization of AJ proteins is unaltered in ZO-depleted cells. (B) Monolayers of control and dKD cells were fixed and stained with antibodies against the indicated AJ proteins; the images are displayed as 1-μm-thick, maximum-density projections of the AJC. Although the characteristic change in cell shape of dKD cells is apparent, the lateral distribution of the core components of the AJs appear similar to those of control cells. Scale bar: 10 μm.

marked disorganization of myosin II staining in the apical domain, which they interpreted as a failure to incorporate myosin II into the perijunctional actin ring (Yamazaki *et al*., 2008). In contrast, we observed that the actomyosin bundles at the AJ in ZO dKD MDCK cells are highly organized and closely associated with the plasma membrane. Furthermore, we did not detect any delay in the localization of E-cadherin to cell–cell contacts following Ca^{2+}-switch (Figure S5B). We do not know the reason for these different observations, but it is possible that this is due to cell type differences.

ZO depletion does not disrupt AJ assembly or cell polarity

Epithelial structure is dictated by a complex interaction between components of the polarity complex and cell–cell adhesion (Nelson, 2009). Polarity proteins regulate the segregation of apical and basal lateral domains and the polarized architecture of the cortical cytoskeleton, while contacts between the cytoskeleton and the cadherin–catenin complex mediate the dynamic changes in epithelial structure during development or wound healing. ZO proteins can interact directly with components of both the polarity and cadherin–catenin complex (Roh *et al*., 2002; Métais *et al*., 2005; Fanning and Anderson, 2009). However, in our study, there were no apparent changes in the distribution of E-cadherin, catenins, or components of the polarity complex, such as PAR3 and aPKC, nor were there any apparent changes in cell polarity or cell–cell adhesion. This suggests that ZO proteins do not contribute directly to AJ assembly or cell polarity. This is consistent with recent genetic evidence from *Drosophila* and *Caenorhabditis elegans*. In both model systems, loss of ZO-1 resulted in disruption of the cytoskeleton associated with AJ, particularly during dynamic reorganization of epithelia during gastrulation (Lockwood *et al*., 2008) or epidermal sheet movements (Choi *et al*., 2011), with little change in the assembly of AJ or epithelial polarization (Choi *et al*., 2011; Djiane *et al*., 2011). Thus ZO proteins most likely act as downstream effectors of the adhesion and polarity complexes, most likely by regulating cytoskeletal assembly and contractility.

ZO proteins regulate the structure of the apical plasma membrane

There is a notable expansion of the apical plasma membrane in ZO-depleted cells. One interpretation of these results is that the membrane is forced outward by hydrostatic pressure following contraction of the ZA. However, we note that the apical expansion observed in dKD cells appears disconnected with the ZA, and begins almost 2–3 μm from the apical cell–cell contacts (see Figure 6B). Furthermore, this apical expansion is not induced by other proteins (e.g., Shroom3, Willin, and Lulu) that induce apical constriction of the AJ (Hildebrand, 2005; Nakajima and Tanoue, 2010; Ishiuchi and Takeichi, 2011). Another possibility is that apical trafficking of membrane vesicles is disrupted—a role for TJ proteins in apical exocytosis is not without precedent. The exocyst complex, which is responsible for polarized trafficking of vesicles to the plasma membrane (Nelson and Yeaman, 2001), is associated with the TJ in polarized cells (Yeaman *et al*., 2004). Thus one possibility is that exocyst trafficking is disrupted in ZO-depleted cells. Investigators have also recently identified a TJ protein, Kibra, which regulates the structure of the apical membrane (Yoshihama *et al*., 2011). As for ZO proteins, loss of Kibra causes a dramatic expansion of the apical plasma membrane without altering cell polarity. Future studies will determine to what extent, if any, these trafficking processes are regulated by ZO proteins.

We suspect that the roles of ZO-1 and -2 in apical organization are not completely redundant. We have previously demonstrated that depletion of ZO-2 in MDCK cells has little, if any, affect on apical cell shape or contractility. In contrast, we and others have previously demonstrated that depletion of ZO-1 alone in epithelial cells can induce increased linearity of junctions and accumulation of F-actin and myosin II (Otani *et al*., 2006; Van Itallie *et al*., 2009). Nevertheless, the changes in ZO-1 single KDs are relatively weak compared with the ZO dKD cells; the single ZO-1 KD is not associated with expansion of the apical domain, marked apical contractility, or the highly ordered arrays of actomyosin. Thus we suspect that both overlapping and nonoverlapping functions of ZO-1 and -2, and perhaps ZO-3, combine to produce the dramatic apical reorganization in dKD cells.

ZO proteins regulate paracellular permeability of epithelia

ZO proteins have been established as critical regulators of TJ structure and function (Umeda *et al*., 2006), and our studies confirm that depletion of ZO proteins disrupts the normal paracellular permeability of MDCK cells. We observed that ZO-depleted cells had a marked increase in the paracellular flux of larger (>4 Å radius) molecules. We note, however, that the apparent effects of ZO depletion in MDCK cells are somewhat attenuated relative to those previously observed in ZO-depleted Eph4 cells (Umeda *et al*., 2006). For example, we found that some, but not all, TJ proteins are redistributed in ZO-depleted MDCK cells, and we detected apparently normal freeze-fracture fibrils characteristic of claudin assembly (Figure S6). Furthermore, while the MDCK dKD cells showed a marked delay in TER development following calcium switch, similar to that observed in ZO-1 and -2 single-KD cells (Umeda *et al*., 2004; McNeil

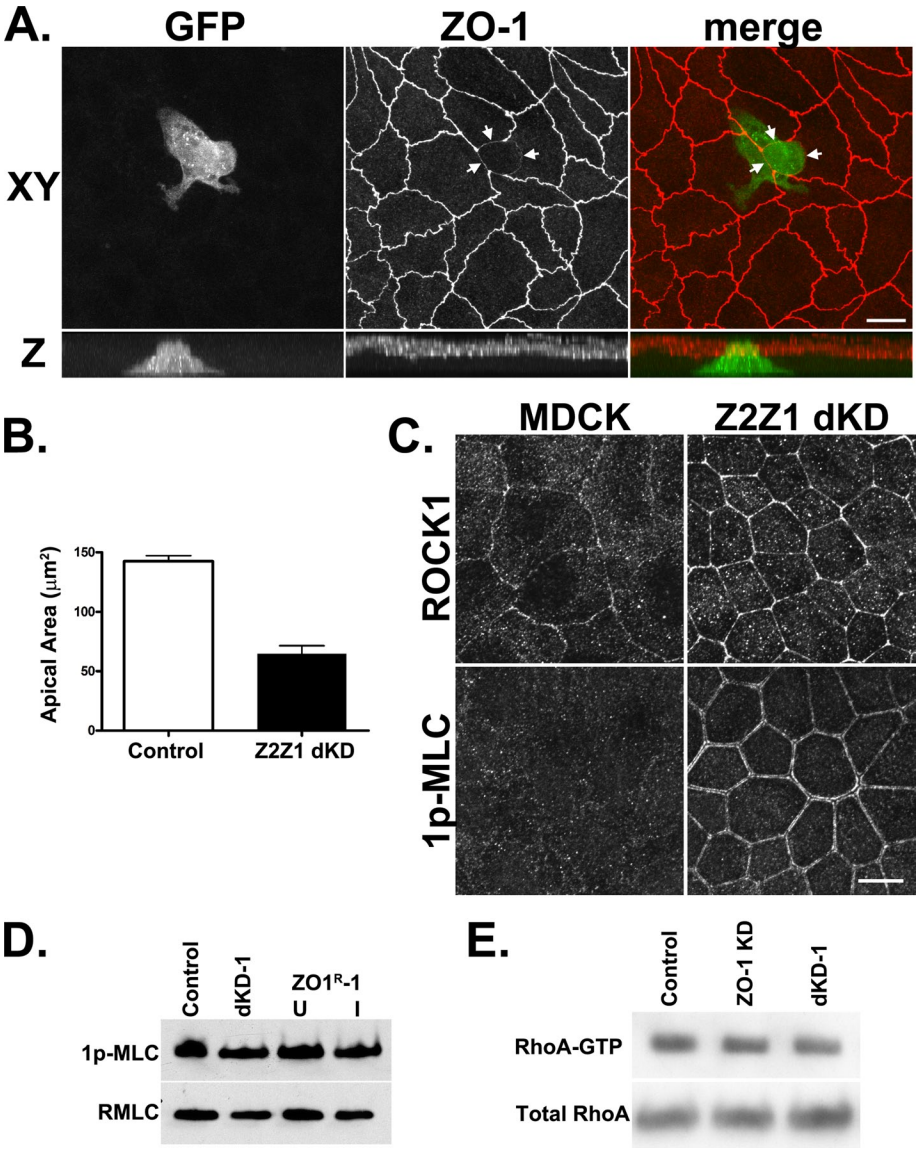

FIGURE 9: ROCK-1 and 1p-MLC are recruited to contractile actomyosin arrays in dKD cells. (A) ZO-depleted cells have a smaller apical diameter than control MDCK cells. dKD cells were transfected with GFP, diluted 1:20 into control MDCK cells, and examined 4 d after plating. The X,Y,Z views are maximum-density projections of the entire confocal volume. Arrows highlight the cell–cell contacts of the ZO-depleted cell with its neighbors. Scale bar: 10 μm. (B) Apical area of control and dKD cells calculated in ImageJ from perimeter traces. Data were compiled from seven different fields, similar to (A). Control, n = 103; Z2Z1 dKD n = 18. (C) Immunocytochemistry of ROCK-1 and 1p-MLC in control and dKD cells. Scale bar: 10 μm. (D) Western blot of 1p-MLC and total regulatory myosin light chain (RMLC) in control, dKD cells, or dKD cells uninduced (U) or induced (I) to express ZO1R. Note that the overall cellular levels of 1p-MLC are unchanged in dKD cells relative to control or ZO1R (U) cells. (E) RhoA-GTP pulldown assay; the cellular levels of RhoA-GTP in control, ZO-1 single-KD, and ZO dKD cells were analyzed using a standard pulldown assay with RBD. Western blots of total RhoA and RBD-bound fractions were stained with antibodies against RhoA.

et al., 2006; Van Itallie *et al.*, 2009), the TER of MDCK dKD cells was indistinguishable from control cells at steady state. This is in a marked contrast to the complete loss of barrier structure and function observed in ZO-depleted Eph4 cells (Umeda *et al.*, 2006). It is likely that the differences we observed are related to cell models used and/or the amplitude of the KD achieved; that is, the Umeda study used homologous recombination to completely remove the ZO-1 gene in Eph4 cells. However, it is also possible the other scaffolding molecules present in TJs, such as MUPP-1, MAGI, or others (reviewed in Guillemot *et al.*, 2008), can partially compensate for the loss of ZO proteins in MDCK cells.

Our results also demonstrate an intriguing uncoupling between ion permeability and larger solute flux, as has been previously observed in other contexts (Balda *et al.*, 1996; Van Itallie *et al.*, 2009, 2010). We found that ion movement (primarily Na^+ and Cl^- in physiological solutions) through claudin-based pores, measured instantaneously by TER, is normal in dKD cells. However, the movement of molecules larger than the pores is dramatically increased. How molecules larger than the pore cross the claudin contacts is poorly understood. One model is that these larger molecules pass through transient breaks in individual strands, and their permeability over time is the sum of movement across several strands in series. Thus changes in the dynamics of strand breaks control the permeability of larger molecules. However, if at least one strand blocks the paracellular space during TER measurement, ion permeability will be properly regulated. It has been proposed that contraction of the perijunctional actomyosin ring might cause such transient breaks (reviewed in Turner, 2009). However, we observed that treatment of dKD cells with blebbistatin, which eliminates the perijunctional actomyosin ring, does not reverse the increased flux of larger molecules seen in ZO-depleted cells. Another alternative is that ZO proteins regulate the membrane dynamics of the claudin proteins. Raleigh and coworkers recently demonstrated that the mobility of claudin-1 in Caco-2 cells was increased in ZO-1 single-KD cells (Raleigh *et al.*, 2011). Thus we propose that ZO proteins regulate paracellular flux by controlling the dynamics of the contacts formed by claudins.

Conclusion

Our data indicate that ZO proteins can cooperatively regulate the apical structure of polarized epithelial cells and suggest that ZO proteins may play a role in the morphogenetic processes that regulate epithelial organ development and repair. Such a role has been previously suggested by both genetic and cell culture studies. For example, loss of ZO-1 in flies and *C. elegans* disrupts epithelial morphogenesis in developmental processes, such as gastrulation, tracheal morphogenesis, and ectodermal sheet migration (Jung *et al.*, 2006; Lockwood *et al.*, 2008; Seppa *et al.*, 2008; Choi *et al.*, 2011). Similarly, depletion of ZO-1 in MDCK cells grown in three-dimensional culture disrupts the formation of epithelial cysts (Sourisseau *et al.*, 2006), although our findings in dKD cells contradict these studies. In fact, the results of our three-dimensional culture experiments are more consistent with invertebrate studies of ZO-1 function. For example, we note that loss

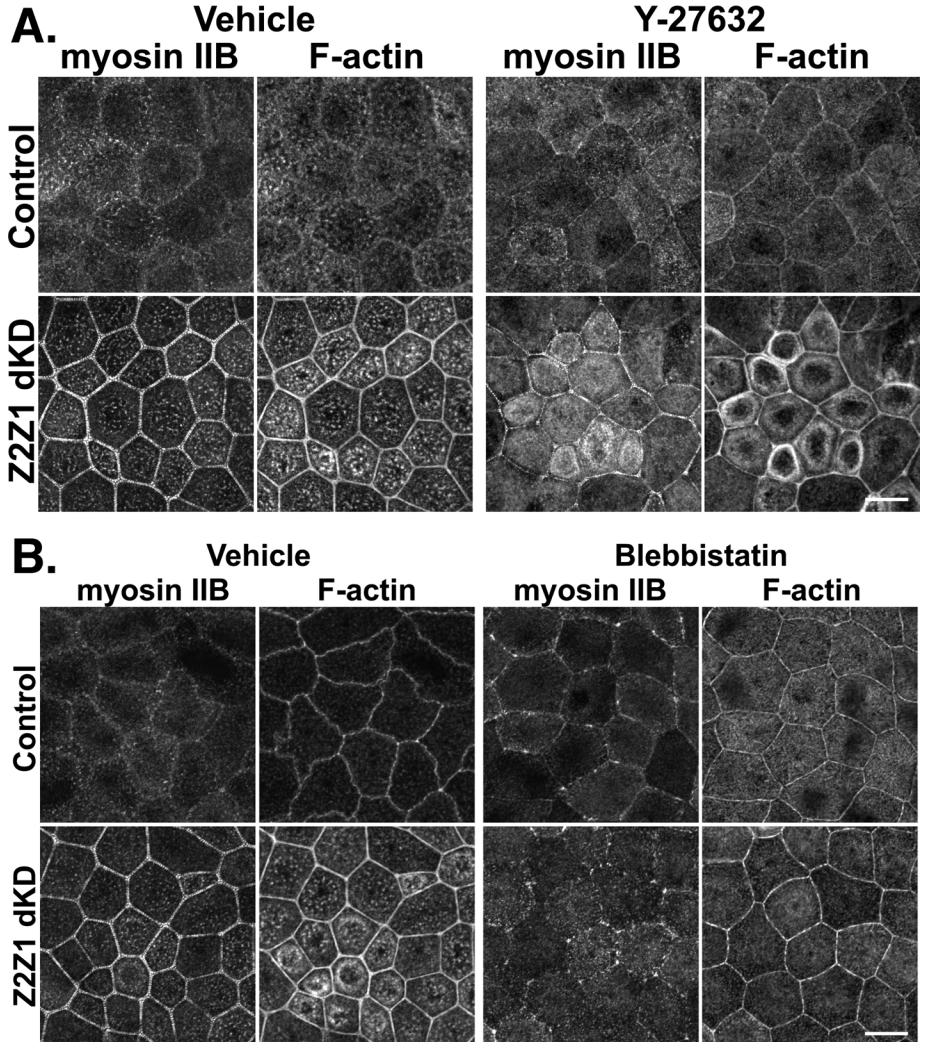

FIGURE 10: Blebbistatin, but not the ROCK inhibitor Y-27632, can reverse the accumulation of actin arrays at the AJC. (A) Monolayers of control and dKD cells were treated with vehicle or 30 μM of the ROCK inhibitor Y-27632 for 15 h and subsequently fixed and stained with TRITC-phalloidin (F-actin) or antibodies specific for myosin IIB. Images are presented as maximum-density projections at the AJC, as described in *Materials and Methods*. (B) As in (A), but monolayers were treated with vehicle or 100 μM blebbistatin. Although there are clear changes in the distribution of F-actin at the AJC, the F-actin/myosin IIB arrays characteristic of dKD cells are still present. In contrast, the actomyosin arrays are absent in the blebbistatin-treated cells. Scale bar: 10 μm.

of ZO protein Pyd in *Drosophila* is not associated with a general failure to form tubular structures. It is instead characterized by changes in the structure of these tubules and the ability of individual cells to properly intercalate with their neighbors (Jung *et al.*, 2006; Choi *et al.*, 2011). Furthermore, in Pyd-null embryos there is a marked deficiency in the migration of epithelial sheets in processes such as dorsal closure. Our preliminary observations suggest that a similar defect in epithelial sheet migration is present in ZO-depleted MDCK II cells, and we will pursue this avenue in future studies. From our current studies, we propose that ZO proteins regulate epithelial morphogenesis, in part, by regulating the assembly and function of cytoskeletal arrays in the AJC. However, ZO proteins have also been implicated in signaling pathways that control cell size, shape, and differentiation during development (Balda *et al.*, 2003; Georgiadis *et al.*, 2010; Djiane *et al.*, 2011; Oka *et al.*, 2012). Future studies will determine to what extent ZO proteins may coordinate signaling and cytoskeletal dynamics during morphogenetic processes.

MATERIALS AND METHODS

Antibodies and reagents

All reagents were purchased from Sigma-Aldrich (St. Louis, MO) unless otherwise indicated. Antibodies and conditions of their use are outlined in Table S1.

Cell lines, expression vectors, and pharmacological manipulation

MDCK Tet-Off cells (clone T23; Clontech, Mountainview, CA) were maintained under standard conditions in complete media: DMEM (high glucose) supplemented with 10% fetal bovine serum, penicillin, and streptomycin. Three-dimensional culture of MDCK cells and immunocytochemical analysis were performed according to previously established protocols (Pollack *et al.*, 1998). All immunocytochemistry and permeability assays were performed on cells cultured on 12-mm- diameter Transwell filter inserts with a 0.4-μm pore size (Corning, Corning, NY). Cells were plated at a density of 10^5 cells/cm^2 and cultured for 10 d, with media changes every 2–3 d. The ZO-1 and -2 single-KD MDCK Tet-Off cells and the pSUPER shRNA constructs used to make them are described elsewhere (Van Itallie *et al.*, 2008). To construct ZO-2/ZO-1 dKD (Z2Z1 dKD) cell lines, a low-passage (pass 2) ZO-2 single-KD cell line was cotransfected with a 1:20 ratio of the plasmid pBlast49 and the previously described pSUPER ZO-1 shRNA construct by the process of Nucleofection (Lonza, Cologne, Germany) using the manufacturer's protocol (Solution L, program L-005, 2 μg total plasmid). Alternatively, ZO-1 single-KD cells were transfected with the pSUPER ZO-2 shRNA constructs to create ZO-1/ZO-2 dKD lines (Z1Z2 dKD). The experimental outcomes were identical regardless of the order of transfection. Stable lines were selected in standard media supplemented with 10 μg/ml blasticidin (InvivoGen, San Diego, CA), and at least three antibiotic-resistant clones were isolated with cloning rings and screened for both ZO-1 and -2 depletion by Western blotting and immunocytochemistry.

To generate a Tet-inducible full-length ZO-1 rescue construct (ZO1R), the previously described pTRE-ZO1myc transgene (Fanning *et al.*, 2007) was modified by QuikChange Multi Site-Directed mutagenesis (Agilent Technologies, Santa Clara, CA) to disrupt the shRNA-binding sites. It was necessary to make conservative mutations at two distinct sites in the myc-tagged ZO-1 transgene to ensure that all possible interactions with the three different shRNA sequences were disrupted. Primer sequences were as follows: 5′-CAATAAAGCAAATCATAGATCAAGACAAGC ACGCATTATTAGATGTAACACCAAATGCAGTTG-3′; 5′-GTCG-C A T G T A G A T C C A A C A A A A G T C T A T A G A A A G G A T C-CATATCCC-3′. The resulting pTRE ZO1R construct was cotransfected with the plasmid pTK-hygro into the Z2Z1 dKD (dKD#3)

cell line, as described above. Clones were selected in 200 μg/ml hygromycin B (Sigma-Aldrich).

To test the role of nonmuscle myosin II and ROCK in the assembly of the AJ cytoskeleton, we treated monolayers of MDCK Tet-Off cells in filter inserts for 15 h with 100 μM blebbistatin, 30 μM of the ROCK inhibitor Y-27635 (InSolution; EMD4Biosciences, Gibbstown, NJ) or an equivalent volume of vehicle (dimethyl sulfoxide) in complete media (described above) and processed the cells for immunocytochemistry as described below.

Epithelial permeability measurements

TER, dilution potential (Colegio *et al.*, 2002), and the flux of polyethylene glycol (Van Itallie *et al.*, 2008) or fluorescein isothiocyanate (FITC)-dextran (Van Itallie *et al.*, 2009) across monolayers are described in detail in the reports indicated. All measurements were performed in triplicate on three different dKD cell lines.

Western blots and RhoA-GTP binding assays

For Western blots, cells were plated at low density in 35-mm dishes and grown for 10 d. The dishes were placed on ice, washed twice in ice-cold phosphate-buffered saline (PBS) supplemented with 1.8 mM $CaCl_2$ (PBS^+), and lysed in 0.25 ml of a lysis buffer containing 62.5 nM Tris, 10% glycerol, and 2% SDS. These lysates were sonicated briefly on ice to disrupt genomic DNA, and the protein concentration was measured using the BCA Protein Assay (Thermo Scientific, Rockford, IL) according to the manufacturer's instructions. Forty micrograms of total lysate was adjusted to a final volume of 20 μl containing 0.3 M β-mercaptoethanol and 0.002% bromophenol blue, heated to 95°C for 3 min, and resolved by SDS–PAGE. Gels were transferred to nitrocellulose filters and then blocked in a solution of PBS and 10% dry milk powder (DMP) for 1 h. Filters were incubated for 2 h in primary antibodies (Table S1) diluted in a solution of PBS, 5% DMP, and 1% Tween-20 (PBS-T); washed four times for 5 min each in PBS-T; and incubated for 30 min with 1:10,000 dilution of the appropriate species-specific secondary antibodies coupled to IRDyes (Rockland, Gilbertsville, MD). After four more washes in PBS-T, filters were imaged with the Odyssey infrared imaging system (Licor Biosciences, Lincoln, NE).

For RhoA-GTP binding assays, a 10-cm dish of cells was washed twice with PBS^+ and lysed in 0.3 ml of Mg^{2+} lysis buffer (50 mM Tris-Cl, 500 mM NaCl, 0.1% SDS, 1% TX-100, 0.5% sodium deoxycholic acid, 10 mM $MgCl_2$, 1 mM sodium orthovanadate and 1 mM NaF; pH 7.6) supplemented with protease inhibitors (Roche Diagnostics, Indianapolis, IN). The lysate was clarified by centrifugation at 20,000 × *g*, and the soluble supernatant was transferred to a new tube containing 50 μg GTPase-binding domain of Rhotekin (GST-RBD) (compliments of Burridge Lab, University of North Carolina, Chapel Hill, NC) bound to glutathione Sepharose (GE Healthcare, Piscataway, NJ). The Sepharose beads were incubated with the lysate for 45 min, washed three times with Mg^{2+} lysis buffer, and resuspended in 20 μl of gel sample buffer. The GST-RBD bound proteins (Figure 9, RhoA-GTP) and ~ 10 μg of the clarified lysate (Figure 9, Total RhoA) were resolved by SDS–PAGE and transferred to Immobilon FL membranes in 25 mM Tris-CL, 192 mM glycine, and 20% methanol for 1 h at 250 mA, and the filters were blocked as described above. The filters were incubated with 1:500 dilution of mouse anti-RhoA primary antibody in PBS-T, which was followed by 1:2000 dilution of horseradish peroxidase–conjugated goat anti–mouse immunoglobulin G (IgG; Jackson Immunoresearch, West Grove, PA), and cells were visualized with enhanced chemiluminescence (Thermo Scientific).

Immunocytochemistry

All filter inserts were washed twice in PBS^+ and fixed for 30 min in ice-cold ethanol. In some cases, cells were initially fixed in 1% (e.g., AF6/afadin, E-cadherin, JAM-A, 1p-MLC, and PAR3) or 4% paraformaldehyde (p120, ezrin) in PBS, washed two times for 10 min each time in PBS, and then permeabilized in a solution of PBS, 0.2% Triton X-100 (EMD Biosciences, San Diego, CA). After two more washes in PBS, filters were excised from the insert with a razor blade, transferred into a 12-well plate, and blocked for 1 h in 5% normal donkey serum (Jackson Immunoresearch) diluted in PBS. All primary and secondary antibodies were diluted in PBS supplemented with 1% IgG-free, protease-free bovine serum albumin (PBS/BSA; Jackson Immunoresearch). Filters were inverted cell-side-down on a 40 μl drop of the appropriate dilution of primary antibody (Table S1) and incubated overnight at 4°C. Filters were transferred back to the 12-well dish and washed three times for 15 min each time in PBS/BSA, and then incubated with the appropriate species-specific affinity-purified secondary antibodies conjugated to Cy2 (1:200 dilution), Cy3 (1:1000), or Cy5 (1:200; Jackson Immunoresearch). F-actin was visualized with 0.4 μg/ml tetramethylrhodamine isothiocyanate (TRITC)-phalloidin (Sigma-Aldrich). Samples were imaged on a Zeiss LSM510 confocal microscope using a 60× Plan Apo lens, and photomultiplier settings were identical for both control and dKD cells to allow direct comparison. Image stacks were acquired through the whole cell volume with a fixed pinhole of 0.7 μm (all channels) and a step size of 0.35 μm. All volumes were originally processed in the LSM image browser (Zeiss, Thornwood, NY), and are presented here as maximum-density projections of 1.05 μm (three frames) centered on the apical surface (as marked by ZO-1, Af-6/afadin, or PAR3 staining) or the substrate-attached surface (just above the filter, marked by autofluorescence).

EM

TEM. Cell monolayers were grown on 12-mm-diameter Transwell polyester (for *x-y* cross-section) or polycarbonate (for en face sections) filter inserts. After 10 d in culture, epithelia were fixed in 3% glutaraldehyde/0.1 sodium cacodylate/0.05 $CaCl_2$ (pH 7.4), for 1 h at room temperature. Following three rinses with sodium cacodylate buffer, the monolayers were postfixed for 45 min in 1% osmium tetroxide/1.25% potassium ferrocyanide/0.1 sodium cacodylate buffer at room temperature (Russel and Burguet, 1977). After washes in deionized water, the cells were stained en bloc with 2% aqueous uranyl acetate for 20 min and dehydrated using increasing concentrations of ethanol (30%, 50%, 75%, 100%, 100%, 10 min each), which was followed by embedment in Polybed 812 epoxy resin (Polysciences, Warrington, PA). For en face sections, the filters were held flat during embedment with Thermanox coverslips, which were then detached prior to sectioning. The monolayers were sectioned either parallel or perpendicular to the substrate at 70 nm using a diamond knife. Ultrathin sections were collected on 200-mesh copper grids and stained with 4% aqueous uranyl acetate for 15 min, and then Reynolds' lead citrate for 7 min (Reynolds, 1963). Samples were viewed using a LEO EM910 transmission electron microscope operating at 80 kV (LEO Electron Microscopy, Thornwood, NY). Digital images were acquired using a Gatan Orius SC1000 CCD Digital Camera and Digital Micrograph 3.11.0 (Gatan, Pleasanton, CA).

SEM. Duplicate cell monolayers were fixed in buffered glutaraldehyde as described in *TEM* for correlative SEM. Following aldehyde fixation, the cells were further stabilized using a modified osmium-tannic acid method (Katsumoto *et al.*, 1981) before dehydration. Briefly, cells were treated with 1% osmium

tetroxide in 0.1 M sodium cacodylate for 30 min, 2% tannic acid in water for 20 min, and 1% osmium tetroxide in water for 20 min at room temperature with water washes between steps. After dehydration with ethanol (as described in *TEM*), the samples were dried in a Samdri-795 (Tousimis Research Corporation, Rockville, MD) critical point dryer using carbon dioxide as the transitional solvent. Filters were mounted on aluminum planchets with double-sided carbon adhesive and coated with a 10-nm thickness of gold–palladium alloy (60Au:40Pd, Hummer X Sputter Coater; Anatech USA, Union City, CA). Specimens were examined using a Zeiss Supra 25 FESEM operating at 5 kV with 10-μm aperture (Carl Zeiss, Peabody, MA).

ACKNOWLEDGMENTS

The authors thank Mark Peifer, Alpha Yap, Keith Burridge, Laurel Rodgers, and members of our laboratories for many thoughtful conversations and/or comments on the manuscript. We also thank Jennifer Holmes and Tanner Beam for technical support; Sandra Citi, Klaus Ebnet, George Ojakian, and Bruce Stevenson for sharing antibodies; and Michael Chua and Neal Kramarcy of the Michael Hooker Microcopy Facility for advice on confocal imaging. We are especially grateful to Erika Wittchen and the Burridge Lab for reagents and advice pertaining to Rho-GTPase assays, to Katy Liu for assistance with 3D culture, and to Victoria Madden and Steven Ray of the Microscopy Services Laboratory at the University of North Carolina, Chapel Hill, for EM. This project was supported by a grant from the National Institute of Diabetes and Digestive and Kidney Diseases (DK061397) to A.S.F. and by intramural funding from the Division of Intramural Research, National Heart, Lung, and Blood Institute, and the Office of the Director, National Institutes of Health (C.M.V.I. and J.M.A.).

REFERENCES

Anderson JM, Van Itallie CM (2009). Physiology and function of the tight junction. Cold Spring Harb Perspect Biol 1, a002584.

Ando-Akatsuka Y, Yonemura S, Itoh M, Furuse M, Tsukita S (1999). Differential behavior of E-cadherin and occludin in their colocalization with ZO-1 during the establishment of epithelial cell polarity. J Cell Physiol 179, 115–125.

Balda MS, Garrett MD, Matter K (2003). The ZO-1–associated Y-box factor ZONAB regulates epithelial cell proliferation and cell density. J Cell Biol 160, 423–432.

Balda MS, Whitney JA, Flores C, González S, Cereijido M, Matter K (1996). Functional dissociation of paracellular permeability and transepithelial electrical resistance and disruption of the apical-basolateral intramembrane diffusion barrier by expression of a mutant tight junction membrane protein. J Cell Biol 134, 1031–1049.

Baum B, Georgiou M (2011). Dynamics of adherens junctions in epithelial establishment, maintenance, and remodeling. J Cell Biol 192, 907–917.

Capaldo CT, Macara IG (2007). Depletion of E-cadherin disrupts establishment but not maintenance of cell junctions in Madin-Darby canine kidney epithelial cells. Mol Biol Cell 18, 189–200.

Chen VC, Li X, Perreault H, Nagy JI (2006). Interaction of zonula occludens-1 (ZO-1) with α-actinin-4: application of functional proteomics for identification of PDZ domain-associated proteins. J Proteome Res 5, 2123–2134.

Choi W, Jung KC, Nelson KS, Bhat MA, Beitel GJ, Peifer M, Fanning AS (2011). The single *Drosophila* ZO-1 protein Polychaetoid regulates embryonic morphogenesis in coordination with Canoe/afadin and Enabled. Mol Biol Cell 22, 2010–2030.

Colegio OR, Van Itallie CM, McCrea HJ, Rahner C, Anderson JM (2002). Claudins create charge-selective channels in the paracellular pathway between epithelial cells. Am J Physiol Cell Physiol 283, C142-C147.

Djiane A, Shimizu H, Wilkin M, Mazleyrat S, Jennings MD, Avis J, Bray S, Baron M (2011). Su(dx) E3 ubiquitin ligase–dependent and –independent functions of Polychaetoid, the *Drosophila* ZO-1 homologue. J Cell Biol 192, 189–200.

Etournay R, Zwaenepoel I, Perfettini I, Legrain P, Petit C, El-Amraoui A (2007). Shroom2, a myosin-VIIa- and actin-binding protein, directly interacts with ZO-1 at tight junctions. J Cell Sci 120, 2838–2850.

Fanning AS, Anderson JM (2009). Zonula occludens-1 and -2 are cytosolic scaffolds that regulate the assembly of cellular junctions. Ann NY Acad Sci 1165, 113–120.

Fanning AS, Little BP, Rahner C, Utepbergenov D, Walther Z, Anderson JM (2007). The unique-5 and -6 motifs of ZO-1 regulate tight junction strand localization and scaffolding properties. Mol Biol Cell 18, 721–731.

Georgiadis A *et al*. (2010). The tight junction associated signalling proteins ZO-1 and ZONAB regulate retinal pigment epithelium homeostasis in mice. PLoS One 5, e15730.

Guillemot L, Paschoud S, Pulimeno P, Foglia A, Citi S (2008). The cytoplasmic plaque of tight junctions: a scaffolding and signalling center. Biochim Biophys Acta 1778, 601–613.

Gumbiner B, Stevenson B, Grimaldi A (1988). The role of the cell adhesion molecule uvomorulin in the formation and maintenance of the epithelial junctional complex. J Cell Biol 107, 1575–1587.

Harris TJC, Tepass U (2010). Adherens junctions: from molecules to morphogenesis. Nat Rev Mol Cell Biol 11, 502–514.

Hartsock A, Nelson WJ (2008). Adherens and tight junctions: structure, function and connections to the actin cytoskeleton. Biochim Biophys Acta 1778, 660–669.

Hernandez S, Chavez Munguia B, Gonzalez-Mariscal L (2007). ZO-2 silencing in epithelial cells perturbs the gate and fence function of tight junctions and leads to an atypical monolayer architecture. Exp Cell Res 313, 1533–1547.

Hildebrand JD (2005). Shroom regulates epithelial cell shape via the apical positioning of an actomyosin network. J Cell Sci 118, 5191–5203.

Huo L, Wen W, Wang R, Kam C, Xia J, Feng W, Zhang M (2011). Cdc42-dependent formation of the ZO-1/MRCKβ complex at the leading edge controls cell migration. EMBO J 30, 665–678.

Ikenouchi J, Umeda K, Tsukita S, Furuse M (2007). Requirement of ZO-1 for the formation of belt-like adherens junctions during epithelial cell polarization. J Cell Biol 176, 779–786.

Inagaki M, Irie K, Deguchi-Tawarada M, Ikeda W, Ohtsuka T, Takeuchi M, Takai Y (2003). Nectin-dependent localization of ZO-1 at puncta adhaerentia junctions between the mossy fiber terminals and the dendrites of the pyramidal cells in the CA3 area of adult mouse hippocampus. J Comp Neurol 460, 514–524.

Ishiuchi T, Takeichi M (2011). Willin and Par3 cooperatively regulate epithelial apical constriction through aPKC-mediated ROCK phosphorylation. Nat Cell Biol 13, 860–866.

Itoh M, Nagafuchi A, Moroi S, Tsukita S (1997). Involvement of ZO-1 in cadherin-based cell adhesion through its direct binding to α catenin and actin filaments. J Cell Biol 138, 181–192.

Ivanov AI, Hunt D, Utech M, Nusrat A, Parkos CA (2005). differential roles for actin polymerization and a myosin II motor in assembly of the epithelial apical junctional complex. Mol Biol Cell 16, 2636–2650.

Ivanov AI, McCall IC, Parkos CA, Nusrat A (2004). Role for actin filament turnover and a myosin ii motor in cytoskeleton-driven disassembly of the epithelial apical junctional complex. Mol Biol Cell 15, 2639–2651.

Jung AC, Ribeiro C, Michaut L, Certa U, Affolter M (2006). Polychaetoid/ZO-1 is required for cell specification and rearrangement during *Drosophila* tracheal morphogenesis. Curr Biol 16, 1224–1231.

Katsumoto T, Naguro T, Iino A, Takagi A (1981). The effect of tannic acid on the preservation of tissue culture cells for scanning electron microscopy. J Electron Microsc (Tokyo) 30, 177–182.

Katsuno T *et al*. (2008). Deficiency of zonula occludens-1 causes embryonic lethal phenotype associated with defected yolk sac angiogenesis and apoptosis of embryonic cells. Mol Biol Cell 19, 2465–2475.

Kausalya PJ, Phua DC, Hunziker W (2004). Association of ARVCF with zonula occludens (ZO)-1 and ZO-2: binding to PDZ-domain proteins and cell-cell adhesion regulate plasma membrane and nuclear localization of ARVCF. Mol Biol Cell 15, 5503–5515.

Kremerskothen J *et al*. (2011). Zona occludens proteins modulate podosome formation and function. FASEB J 25, 505–514.

Lockwood C, Zaidel-Bar R, Hardin J (2008). The *C. elegans* zonula occludens ortholog cooperates with the cadherin complex to recruit actin during morphogenesis. Curr Biol 18, 1333–1337.

Martinez-Palomo A, Meza I, Beaty G, Cereijido M (1980). Experimental modulation of occluding junctions in a cultured transporting epithelium. J Cell Biol 87, 736–745.

Mattagajasingh SN, Huang S-C, Hartenstein JS, Benz EJ (2000). Characterization of the interaction between protein 4.1R and ZO-2. J Biol Chem 275, 30573–30585.
McNeil E, Capaldo CT, Macara IG (2006). Zonula occludens-1 function in the assembly of tight junctions in Madin-Darby canine kidney epithelial cells. Mol Biol Cell 17, 1922–1932.
Métais J-Y, Navarro C, Santoni M-J, Audebert S, Borg J-P (2005). hScrib interacts with ZO-2 at the cell-cell junctions of epithelial cells. FEBS Lett 579, 3725–3730.
Mooseker MS (1976). Brush border motility. Microvillar contraction in triton-treated brush borders isolated from intestinal epithelium. J Cell Biol 71, 417–433.
Nakajima H, Tanoue T (2010). Epithelial cell shape is regulated by Lulu proteins via myosin-II. J Cell Sci 123, 555–566.
Nelson WJ (2009). Remodeling epithelial cell organization: transitions between front–rear and apical–basal polarity. Cold Spring Harb Perspect Biol 1, DOI: 10.1101/cshperspect.a000513.
Nelson WJ, Yeaman C (2001). Protein trafficking in the exocytic pathway of polarized epithelial cells. Trends Cell Biol 11, 483–486.
Niessen CM, Leckband D, Yap AS (2011). Tissue organization by cadherin adhesion molecules: dynamic molecular and cellular mechanisms of morphogenetic regulation. Physiol Rev 91, 691–731.
Nishimura T, Takeichi M (2008). Shroom3-mediated recruitment of Rho kinases to the apical cell junctions regulates epithelial and neuroepithelial planar remodeling. Development 135, 1493–1502.
Oka T, Schmitt AP, Sudol M (2012). Opposing roles of angiomotin-like-1 and zona occludens-2 on pro-apoptotic function of YAP. Oncogene 31, 128–134.
Otani T, Ichii T, Aono S, Takeichi M (2006). Cdc42 GEF Tuba regulates the junctional configuration of simple epithelial cells. J Cell Biol 175, 135–146.
Pollack AL, Runyan RB, Mostov KE (1998). Morphogenetic mechanisms of epithelial tubulogenesis: MDCK cell polarity is transiently rearranged without loss of cell–cell contact during scatter factor/hepatocyte growth factor-induced tubulogenesis. Dev Biol 204, 64–79.
Pulimeno P, Paschoud S, Citi S (2011). A Role for ZO-1 and PLEKHA7 in recruiting paracingulin to tight and adherens junctions of epithelial cells. J Biol Chem 286, 16743–16750.
Raleigh DR *et al*. (2011). Occludin S408 phosphorylation regulates tight junction protein interactions and barrier function. J Cell Biol 193, 565–582.
Reynolds ES (1963). The use of lead citrate at high pH as an electron-opaque stain in electron microscopy. J Cell Biol 17, 208–212.
Roh MH, Liu C-J, Laurinec S, Margolis B (2002). The carboxyl terminus of zona occludens-3 binds and recruits a mammalian homologue of Discs lost to tight junctions. J Biol Chem 277, 27501–27509.
Russel L, Burguet S (1977). Ultrastructure of Leydig cells as revealed by secondary tissue treatment with a ferrocyanide-osmium mixture. Tissue Cell 9, 751–766.
Seppa MJ, Johnson RI, Bao S, Cagan RL (2008). Polychaetoid controls patterning by modulating adhesion in the *Drosophila* pupal retina. Dev Biol 318, 1–16.
Shen L, Weber CR, Raleigh DR, Yu D, Turner JR (2011). Tight junction pore and leak pathways: a dynamic duo. Annu Rev Physiol 73, 283–309.
Smutny M, Cox HL, Leerberg JM, Kovacs EM, Conti MA, Ferguson C, Hamilton NA, Parton RG, Adelstein RS, Yap AS (2010). Myosin II isoforms identify distinct functional modules that support integrity of the epithelial zonula adherens. Nat Cell Biol 12, 696–702.
Sourisseau T, Georgiadis A, Tsapara A, Ali RR, Pestell R, Matter K, Balda MS (2006). Regulation of PCNA and cyclin D1 expression and epithelial morphogenesis by the ZO-1-regulated transcription factor ZONAB/DbpA. Mol Cell Biol 26, 2387–2398.
Suzuki A, Ishiyama C, Hashiba K, Shimizu M, Ebnet K, Ohno S (2002). aPKC kinase activity is required for the asymmetric differentiation of the premature junctional complex during epithelial cell polarization. J Cell Sci 115, 3565–3573.
Takahashi K, Matsuo T, Katsube T, Ueda R, Yamamoto D (1998). Direct binding between two PDZ domain proteins Canoe and ZO-1 and their roles in regulation of the jun N-terminal kinase pathway in Drosophila morphogenesis. Mech Dev 78, 97–111.
Tsukita S, Katsuno T, Yamazaki Y, Umeda K, Tamura A (2009). Roles of ZO-1 and ZO-2 in establishment of the belt-like adherens and tight junctions with paracellular permselective barrier function. Ann NY Acad Sci 1165, 44–52.
Turner JR (2009). Intestinal mucosal barrier function in health and disease. Nat Rev Immunol 9, 799–809.
Umeda K, Ikenouchi J, Katahira-Tayama S, Furuse K, Sasaki H, Nakayama M, Matsui T, Tsukita S, Furuse M (2006). ZO-1 and ZO-2 independently determine where claudins are polymerized in tight-junction strand formation. Cell 126, 741–754.
Umeda K, Matsui T, Nakayama M, Furuse K, Sasaki H, Furuse M, Tsukita S (2004). Establishment and characterization of cultured epithelial cells lacking expression of ZO-1. J Biol Chem 279, 44785–44794.
Van Itallie CM, Fanning AS, Bridges A, Anderson JM (2009). ZO-1 stabilizes the tight junction solute barrier through coupling to the perijunctional cytoskeleton. Mol Biol Cell 20, 3930–3940.
Van Itallie CM, Fanning AS, Holmes J, Anderson JM (2010). Occludin is required for cytokine-induced regulation of tight junction barriers. J Cell Sci 123, 2844–2852.
Van Itallie CM, Holmes J, Bridges A, Gookin JL, Coccaro MR, Proctor W, Colegio OR, Anderson JM (2008). The density of small tight junction pores varies among cell types and is increased by expression of claudin-2. J Cell Sci 121, 298–305.
Wei X, Ellis HM (2001). Localization of the Drosophila MAGUK protein Polychaetoid is controlled by alternative splicing. Mech Dev 100, 217–231.
Wittchen ES, Haskins J, Stevenson BR (2003). NZO-3 expression causes global changes to actin cytoskeleton in Madin-Darby canine kidney cells: linking a tight junction protein to Rho GTPases. Mol Biol Cell 14, 1757–1768.
Xu J, Kausalya PJ, Phua DC, Ali SM, Hossain Z, Hunziker W (2008). Early embryonic lethality of mice lacking ZO-2, but not ZO-3, reveals critical and nonredundant roles for individual zonula occludens proteins in mammalian development. Mol Cell Biol 28, 1669–1678.
Yamamoto T, Harada N, Kano K, Taya S-i, Canaani E, Matsuura Y, Mizoguchi A, Ide C, Kaibuchi K (1997). The Ras target AF-6 interacts with ZO-1 and serves as a peripheral component of tight junctions in epithelial cells. J Cell Biol 139, 785–795.
Yamazaki Y, Umeda K, Wada M, Nada S, Okada M, Tsukita S, Tsukita S (2008). ZO-1- and ZO-2-dependent integration of myosin-2 to epithelial zonula adherens. Mol Biol Cell 19, 3801–3811.
Yeaman C, Grindstaff KK, Nelson WJ (2004). Mechanism of recruiting Sec6/8 (exocyst) complex to the apical junctional complex during polarization of epithelial cells. J Cell Sci 117, 559–570.
Yonemura S, Itoh M, Nagafuchi A, Tsukita S (1995). Cell-to-cell adherens junction formation and actin filament organization: similarities and differences between non-polarized fibroblasts and polarized epithelial cells. J Cell Sci 108, 127–142.
Yoshihama Y, Sasaki K, Horikoshi Y, Suzuki A, Ohtsuka T, Hakuno F, Takahashi S-I, Ohno S, Chida K (2011). KIBRA suppresses apical exocytosis through inhibition of aPKC kinase activity in epithelial cells. Curr Biol 21, 705–711.